NEUROSCIENCE
RESEARCH ARTICLE
A. Moutal et al. / Neuroscience 381 (2018) 79–90

CRMP2–Neurofibromin Interface Drives NF1-related Pain

Aubin Moutal,[a] Li Sun,[d†] Xiaofang Yang,[a†] Wennan Li,[a†] Song Cai,[a] Shizhen Luo[a] and Rajesh Khanna[a,b,c*]

[a] *Department of Pharmacology, College of Medicine, University of Arizona, Tucson, AZ, USA*

[b] *Department of Anesthesiology, College of Medicine, University of Arizona, Tucson, AZ, USA*

[c] *Neuroscience Graduate Interdisciplinary Program, College of Medicine, University of Arizona, Tucson, AZ, USA*

[d] *Department of Neurology and Neuroscience Center, The First Hospital of Jilin University, Xinmin Street 71#, Changchun 130021, China*

Abstract—An understudied symptom of the genetic disorder Neurofibromatosis type 1 (NF1) is chronic idiopathic pain. We used targeted editing of *Nf1* in rats to provide direct evidence of a causal relationship between neurofibromin, the protein product of the *Nf1* gene, and pain responses. Our study data identified a protein-interaction network with collapsin response meditator protein 2 (CRMP2) as a node and neurofibromin, syntaxin 1A, and the N-type voltage-gated calcium (CaV2.2) channel as interaction edges. Neurofibromin uncouples CRMP2 from syntaxin 1A. Upon loss/mutation of neurofibromin, as seen in patients with NF1, the CRMP2/Neurofibromin interaction is uncoupled, which frees CRMP2 to interact with both syntaxin 1A and CaV2.2, culminating in increased release of the pro-nociceptive neurotransmitter calcitonin gene-related peptide (CGRP). Our work also identified the CRMP2-derived peptide CNRP1, which uncoupled CRMP2's interactions with neurofibromin, syntaxin 1A, as well as CaV2.2. Here, we tested if CRISPR/Cas9-mediated editing of the *Nf1* gene, which leads to functional remodeling of peripheral nociceptors through effects on the tetrodotoxin-sensitive (TTX-S) Na^+ voltage-gated sodium channel (NaV1.7) and CaV2.2, could be affected using CNRP1, a peptide designed to target the CRMP2–neurofibromin interface. The data presented here shows that disrupting the CRMP2–neurofibromin interface is sufficient to reverse the dysregulations of voltage-gated ion channels and neurotransmitter release elicited by *Nf1* gene editing. As a consequence of these effects, the CNRP1 peptide reversed hyperalgesia to thermal stimulation of the hindpaw observed in *Nf1*-edited rats. Our findings support future pharmacological targeting of the CRMP2/neurofibromin interface for NF1-related pain relief.

Key words: CRMP2, neurofibromin, pain, CaV2.2, NaV1.7, Neurofibromatosis type 1.

INTRODUCTION

Chronic idiopathic pain is a major symptom and comorbidity factor in the neurological disorder Neurofibromatosis type 1 (NF1) (Creange et al., 1999; Drouet et al., 2004). The prevalence of pain in NF1 patients is unknown but qualities of life-based questionnaires consistently identify both the intensity and quality of pain as having a major impact on NF1 patients (Wolkenstein et al., 2001; Ferner, 2007; Kodra et al., 2009; Crawford et al., 2015; Wolters et al., 2015; Bicudo et al., 2016; Ferner et al., 2017; Riklin et al., 2017). The first direct evidence of a causal relationship between neurofibromin, a protein encoded by the *Nf1* gene, and pain responses was demonstrated using a genome-editing approach *in vivo* (Moutal et al., 2017a,f). The truncation of neurofibromin by targeting exon 39 on the *Nf1* gene in sensory neurons, with a specific guide RNA (gRNA) conjugated to clustered regularly interspaced short palindromic repeats (CRISPR) associated protein-9 nuclease (Cas9), resulted in hyperalgesia (Moutal et al., 2017a,f). The underlying mechanism for the observed painful behaviors was hypothesized via remodeling of small-diameter nociceptive sensory neurons (Moutal et al., 2017b). Data from recent studies of rat neurons from Cas9-edited *Nf1* were in agreement with observations in haploinsufficient ($Nf1^{+/-}$) mouse sensory neurons: upregulation of voltage-gated ion channels (Duan et al., 2014; Wang et al., 2010a,b; Moutal et al., 2017a,b,f). Specifi-

*Corresponding author. Address: Department of Pharmacology, College of Medicine, University of Arizona, 1501 North Campbell Drive, P.O. Box 245050, Tucson, AZ 85724, USA.
E-mail address: rkhanna@email.arizona.edu (R. Khanna).

† These authors contributed equally to this work.

Abbreviations: ANOVA, analysis of variance; AP, action potential; Cas9, CRISPR-associated protein-9 nuclease; CaV2.2, N-type voltage-gated calcium channel; CGRP, calcitonin gene-related peptide; CNRP1, CRMP2–neurofibromin regulating peptide 1; CRISPR, clustered regularly interspaced short palindromic repeats; CRMP2, collapsin response mediator protein 2; DMEM, Dulbecco's Modified Eagle's medium; DRG, Dorsal Root Ganglia; EPM, elevated plus maze; gRNA, guide RNA; NaV1.7, Na^+ voltage-gated sodium channel 1.7; NF1, Neurofibromatosis type 1; PPIs, protein–protein interactions; TTX-R, tetrodotoxin-resistant; TTX-S, tetrodotoxin-sensitive.

https://doi.org/10.1016/j.neuroscience.2018.04.002
0306-4522/

cally, the nociceptive synapse in these rodent models of NF1 is characterized by increases in N-type voltage-gated calcium (CaV2.2) as well as tetrodotoxin-sensitive (TTX-S) voltage-gated sodium (NaV1.7) currents (Chew and Khanna, 2018; Duan et al., 2014; Moutal et al., 2017f; Wang et al., 2010a,b). A consequence of this nociceptor remodeling was a reduction in rheobase (i.e., the current required to elicit the first action potential (AP)) and a concomitant increase in excitability (Wang et al., 2005, 2010b; Moutal et al., 2017f). It follows then, that release of excitatory transmitter – calcitonin gene-related peptide (CGRP) – to the spinal dorsal horn was also increased in both *Nf1*-edited rats and *Nf1*$^{+/-}$ mice (Hingtgen et al., 2006; Moutal et al., 2017a). Thus, in NF1, the sensory neurons are primed at the synaptic level for facilitated nociceptive signal transmission. Further studies identified the dysregulation of the collapsin response mediator protein 2 (CRMP2) (Patrakitkomjorn et al., 2008) to be responsible for NF1-related pain.

CRMP2 was initially described as an axonal protein involved in axon guidance and growth (Goshima et al., 1995; Kamata et al., 1998; Fukata et al., 2002). The functional association of neurofibromin and CRMP2 was reported to be essential for neuronal cell differentiation; lack of expression or abnormal regulation of neurofibromin resulted in impaired function of neuronal cells (Lin and Hsueh, 2008; Patrakitkomjorn et al., 2008). Suppression of neurofibromin using neurofibromin small-interfering RNA significantly inhibited neurite outgrowth and upregulated CRMP2 phosphorylation by kinases identified as Cdk5, GSK-3β, and Rho kinase (Patrakitkomjorn et al., 2008). Truncation of the C-terminus of neurofibromin, where CRMP2 binds (Patrakitkomjorn et al., 2008), lead to upregulation of CRMP2 functions in ion channel trafficking (Moutal et al., 2017a,f). CRMP2 binds to and regulates the membrane localization of both CaV2.2 (Brittain et al., 2009, 2011,; Moutal et al., 2016a,b,c) and NaV1.7 (Dustrude et al., 2013, 2016, 2017). CRMP2 also participates in neurotransmitter release (Chi et al., 2009; Moutal et al., 2016b,e). Recent proteomic analysis identified syntaxin 1A as a novel CRMP2-binding protein whose interaction with CRMP2 was strengthened in neurofibromin-depleted cells (Moutal et al., 2017e). These mutually exclusive interactions appear to form a 'core complex' that can facilitate nociceptive transmission in NF1. A peptide targeting CRMP2's interaction domain with neurofibromin, designated CRMP2–neurofibromin regulating peptide 1 (CNRP1,) inhibited CGRP release and acute and neuropathic nociceptive behaviors (Moutal et al., 2017e).

Although an obligatory role for CRMP2 has been established for manifestation of NF1-related pain (Moutal et al., 2017a), the precise manner by which neurofibromin's interaction with CRMP2 leads to alterations in ion channel function is unclear. Here, we tested if targeting the CRMP2/neurofibromin interaction in *Nf1* edited in sensory neurons could reverse ion channel dysregulation, sensory neuron excitability, and hyperalgesia. Our data show that the CNRP1 peptide from CRMP2 is sufficient to reverse alterations of sensory neurons and nociceptive behaviors in NF1without producing motor impairment or anxiety.

EXPERIMENTAL PROCEDURES

Animals

Pathogen-free, adult male and female Sprague–Dawley rats (150–200 g; Harlan Laboratories) were housed in temperature- (23 ± 3 °C) and light (12-h light/12-h dark cycle; lights on 07:00–19:00)-controlled rooms with standard rodent chow and water available *ad libitum*. The Institutional Animal Care and Use Committee of the College of Medicine at the University of Arizona approved all experiments. All procedures were conducted in accordance with the Guide for Care and Use of Laboratory Animals published by the National Institutes of Health and the ethical guidelines of the International Association for the Study of Pain. Animals were randomly assigned to treatment or control groups for the behavioral experiments. Animals were initially housed three per cage but individually housed after the intrathecal cannulation on a 12-h light–dark cycle with food and water *ad libitum*. All behavioral experiments were performed by experimenters who were blinded to the experimental groups and treatments.

Materials

t-CNRP1 peptide (tat cell penetrating peptide sequence: YGRKKRRQRRR fused to CNRP1: HVTEGSGRYIPRKPF) (Moutal et al., 2017e) was synthesized and HPLC-purified (> 95% purity) by Genscript Inc. (Piscataway, NJ, USA). Scramble and random sequence-based peptides conjugated to various cargoes as controls have been previously studied as controls in molecular, biochemical and behavioral assays and demonstrated to have no effects (Brittain et al., 2011; Ju et al., 2012; Piekarz et al., 2012; Francois-Moutal et al., 2015). All chemicals, unless noted were purchased from Sigma (St. Louis, MO, USA). Antibodies were purchased as follows: anti-CaV2.2 polyclonal antibody (Cat# TA308673, Origene Technologies, Inc, Rockville, MD, USA), anti-NaV1.7 (Cat# 75-103, NeuroMab, Davis, CA, USA) or anti-neurofibromin C-terminal (Abcam Cat# ab17963).

gRNA strategy for Nf1 gene targeting

Our strategy to truncate neurofibromin focused on targeting exon 39 of the *Nf1* gene using a guide RNA (gRNA) as described previously (Moutal et al., 2017a,f). We targeted this exon to express a C-terminally truncated neurofibromin protein, since 80% of NF1 patients express a C-terminally truncated neurofibromin (Esposito et al., 2015). The gRNA sequence (GGCAGTAACCCTTTGTC GTT) was inserted into the *BbsI* restriction site of the pSpCas9(BB)-2A-GFP plasmid (PX458, Cat#48138, Addgene, Cambridge, MA) (Ran et al., 2013), a plasmid that allows for simultaneous expression of (i) the Cas9 enzyme; (ii) the gRNA; and (iii) a green fluorescent protein (GFP) – to control for transfection efficiency. All plasmids were verified by Sanger sequencing (Eurofins, Louisville, KY).

Culturing and transfection of rat primary Dorsal Root Ganglia (DRG) Neurons

Rat DRG neurons were isolated from 150- to 174-g Sprague–Dawley rats and then transfected exactly as previously described (Brittain et al., 2011). In brief, removing dorsal skin and muscle and cutting the vertebral bone processes parallel to the dissection stage exposed DRGs. DRGs were then collected, trimmed at their roots, and digested in 3 ml bicarbonate-free, serum-free, sterile Dulbecco's Modified Eagle's medium (DMEM; Cat# 11965, Thermo Fisher Scientific, Waltham, MA, USA) solution containing neutral protease (3.125 mg·ml^{-1}, Cat#LS02104, Worthington, Lakewood, NJ) and collagenase Type I (5 mg·ml^{-1}, Cat# LS004194, Worthington, Lakewood, NJ, USA) and incubated for 45 min at 37 °C under gentle agitation. Dissociated DRG neurons (~1.5 × 10^{6}) were then gently centrifuged to collect cells and washed with DRG media: DMEM containing 1% penicillin/streptomycin sulfate from 10,000 μg/ml stock, 30 ng·ml^{-1} nerve growth factor, and 10% fetal bovine serum (Hyclone). The pelleted cells were re-suspended in Nucleofector transfection reagent containing plasmids. Then, cells were subjected to electroporation protocol O-003 in an Amaxa Biosystem (Lonza, Basel, Switzerland) and plated onto poly-D-lysine- and laminin-coated glass (12- or 15-mm) coverslips. Transfection efficiencies were routinely between 20% and 30% with about ~10% cell death. Small diameter (~ < 30 μm) neurons were selected to target Aδ- and C-fiber nociceptive neurons. All cultures were used within 48 h after transfection.

Patch-clamp electrophysiology

Recordings were obtained from acutely dissociated DRG neurons as described (Moutal et al., 2017e,f; Dustrude et al., 2016). To isolate calcium currents, Na^+ and K^+ currents were blocked with 500 nM TTX (Alomone Labs) and 30 mM tetraethylammonium chloride (Sigma). Extracellular recording solution (at ~310 mOsm) consisted of the following (in millimolar): 110 N-methyl-D-glucamine, 10 $BaCl_2$, 30 tetraethylammonium chloride, 10 HEPES, 10 glucose, pH at 7.4, 0.001 TTX, and 0.01 nifedipine. The intracellular recording solution (at ~310 mOsm) consisted of the following (in millimolar): 150 $CsCl_2$, 10 HEPES, 5 Mg-ATP, 5 BAPTA, pH at 7.4. To isolate the contributions of N-type (CaV2.2) channels, we used the following subunit-selective blockers (all purchased from Alomone Labs, Jerusalem): Nifedipine (10 μM, L-type); ω-agatoxin GIVA (200 nM, P/Q-type) (Mintz et al., 1992); SNX-482 (200 nM, R-type) (Newcomb et al., 1998); and 3,5-dichloro-N-[1-(2,2-dimethyl-tetrahydro-pyran-4-ylmethyl)-4-fluoro-piperidin-4-ylmethyl]-benzamide (TTA-P2, 1 μM, T-type) (Choe et al., 2011).

Whole-cell voltage-clamp and current-clamp recordings were performed at room temperature using an EPC 10 Amplifier-HEKA as previously described (Dustrude et al., 2013). The internal solution for voltage-clamp sodium current recordings contained (in mM): 140 CsF, 1.1Cs-EGTA, 10 NaCl, and 15 HEPES (pH 7.3, 290–310 mOsm/L) and external solution contained (in mM): 140 NaCl, 3 KCl, 30 tetraethylammonium chloride, 1 $CaCl_2$, 0.5 $CdCl_2$, 1 $MgCl_2$, 10 D-glucose, 10 HEPES (pH 7.3, 310–315 mosM/L). For DRG current-clamp experiments the internal solution contained (in mM): 140 KCl, 10 NaCl, 1 $MgCl_2$, 1 EGTA, 10 HEPES (pH 7.2), and 1 ATP-Mg (pH 7.3, 285–295 mOsm/L) and external solution contained (in mM): 154 NaCl, 5.6 KCl, 2 $CaCl_2$, 2.0 $MgCl_2$, 1.0 Glucose, and 10 HEPES (pH 7.4, 305–315 mOsm/L).

DRG neurons were subjected to current–density (I–V) and fast-inactivation voltage protocols. In the I–V protocol, cells were held at a −80 mV holding potential prior to depolarization by 20-ms voltage steps from −70 mV to +60 mV in 5-mV increments. This allowed for collection of current density data to analyze activation of sodium channels as a function of current versus voltage and also peak current density which was typically observed near ~0–10 mV and normalized to cell capacitance (pF). In the fast-inactivation protocol, cells were held at a −80-mV holding potential prior to hyperpolarizing and repolarizing pulses for 500 ms between −120 mV and −10 mV in 5-mV increments. This step conditioned various percentages of channels into fast-inactivated states so that a 0-mV test pulse for 20 ms could reveal relative fast inactivation normalized to maximum current. DRGs were subjected to current–density (I–V) protocol and H-infinity (pre-pulse inactivation protocol). To estimate TTX-R contributions, I–V protocol was run after 10-min incubation with 500 nM TTX. Following holding at −100 mV, 200-ms voltage steps from −70 mV to +60 mV in 5-mV increments allowed for analysis of peak currents. Small and medium diameter DRG neurons which homogenously present TTX-S, TTX-R Na^+ currents (Roy and Narahashi, 1992) and N-type Ca^{2+} currents (Scroggs and Fox, 1992), were selected for all recordings.

Fire-polished recording pipettes with 2–5 megaohms (mΩ) resistances were used for all recordings. Whole-cell recordings were obtained using a HEKA EPC-10 USB (HEKA Instruments Inc, Bellmore, NY, USA); data were acquired using a Patchmaster (HEKA) and analyzed with a Fitmaster (HEKA). Capacitive artifacts were fully compensated, and series resistance was compensated by ~70%. Recordings made from cells with greater than a 5-mV shift in series resistance compensation error were excluded from analysis. All experiments were performed at room temperature (~23 °C).

Confocal imaging

Immunocytochemistry was performed on DRGs that were transfected as described before (Moutal et al., 2017f). Briefly, cells were fixed using 4% paraformaldehyde, 4% sucrose for 20 min at room temperature. Permeabilization was achieved with a 30-min incubation in phosphate-buffered saline (PBS) containing 0.1% Triton X-100, following which nonspecific binding sites were saturated by PBS containing 3% BSA for 30 min. Cell staining was performed with primary antibodies in PBS with 3% BSA overnight at 4 °C. Cells were then washed three times in PBS and incubated with PBS containing 3% BSA and secondary antibodies (Alexa 488 goat anti-mouse and Alexa

594 goat anti-rabbit from Life Technologies, Carlsbad, CA, USA) for 1 h at room temperature. Immunofluorescent micrographs were acquired on a Nikon C1si scanning confocal microscope using CFI Plan APO VC ×60 oil immersion objective with 1.4 numerical aperture. Camera gain and other relevant settings were kept constant. Membrane to cytosol ratio was determined by defining regions of interest on the cytosol and the membrane of each cell using Image J. Total fluorescence intensity was normalized to the area of the region of interest before calculating the membrane to cytosol ratio. Raw images were used for quantification while representative pictures were background subtracted and contrast enhanced for better visualization of the reader.

Implantation of intrathecal catheter

For intrathecal drug administration, rats were chronically implanted with catheters as described by Yaksh and Rudy (Yaksh and Rudy, 1976). Rats were anesthetized with halothane and placed in a stereotactic head holder. The occipital muscles were separated from their occipital insertion and retracted caudally to expose the cisternal membrane at the base of the skull. Polyethylene tubing was passed caudally from the cisterna magna to the level of the lumbar enlargement. Animals were allowed to recover and were examined for evidence of neurologic injury. Animals with evidence of neuromuscular deficits were excluded.

In vivo transfection of CRISPR plasmids

For *in vivo* transfection, the plasmids pSpCas9(BB)-2A-GFP-*Nf1*-gRNA or pSpCas9(BB)-2A-GFP-*Nf1*-control-gRNA were diluted to 0.5 μg/μl in 5% sterile glucose solution. Then, Turbofect *in vivo* transfection reagent (Cat#R0541, Thermo Fisher Scientific, Waltham, MA) was added following manufacturer's instructions. Finally, 20 μL of the plasmid complexes were injected intrathecally in Sprague–Dawley rats.

Immunohistofluorescence and epifluorescence imaging

L5 DRGs were dissected from adult rats and then fixed using 4% paraformaldehyde for 4 h at room temperature (RT). DRGs were next transferred into a 30% sucrose solution and left at 4 °C until sinking of the tissues could be observed (~3 days). Tissues were cut at 10-μm thickness using the Bright OTF 5000 Microtome Cryostat (Hacker Instruments and Industries, Inc., Winnsboro, SC), and fixed onto gelatin-coated glass slides and kept at −20 °C until use. DRG slices were permeabilized and saturated using PBS containing 3% BSA, 0.1% triton X-100 solution for 30 min at RT, and then anti-neurofibromin C-terminal (Abcam Cat# ab17963) was added overnight. The slices were then washed 3X in PBS, and incubated with PBS containing 3% BSA, 0.1% triton X-100 containing secondary antibody (Alexa 594 goat anti-rabbit (Life Technologies)) for at least 3 h at RT. After 3 washes (PBS, 10 min, RT), either DAPI was used to stain the nuclei of cells. Slides were mounted and stored at 4 °C until analysis. Immunofluorescent micrographs were acquired on an Olympus BX51 microscope with a Hamamatsu C8484 digital camera using a 20X UplanS Apo 0.75 numerical aperture objective. For a given experiment, all images were taken using identical acquisition parameters by individuals blinded to the treatment groups.

Measurement of thermal withdrawal latency

The method of Hargreaves et al. (1988) was used. Rats were acclimated within Plexiglas enclosures on a clear glass plate maintained at 30 °C. A radiant heat source (high-intensity projector lamp) was focused onto the plantar surface of the hind paw. When the paw was withdrawn, a motion detector halted the stimulus and a timer. A maximal cutoff of 33.5 s was used to prevent tissue damage.

Elevated plus maze (EPM)

The EPM consists of four elevated (50 cm) arms (50 cm long and 10 cm wide) with two opposing arms containing 30-cm high opaque walls. EPM testing occurred in a quiet testing room with ambient lighting at ~500 lux. On day of testing, rats were allowed to acclimate to the testing room for 20 min. Each rat was placed in a closed arm, facing the enter platform and cage mates started in the same closed arm. Each rat was allowed 5 min to explore the EPM and then returned to its home cage. Between animals the EPM was cleaned thoroughly with Versa-Clean (Fisher Scientific). EPM performance was recorded using an overhead video camera (MHD Sport 2.0 WiFi Action Camera, Walmart.com) for later quantification. Open and closed arm entries were defined as the front two paws entering the arm, and open arm time began the moment the front paws entered the open arm and ended upon exit. An anxiety index was also calculated; the index combines EPM parameters into one unified ratio with values ranging from 0 to 1, with a higher value indicating increased anxiety (Huynh et al., 2011). The following equation was used for calculation of the anxiety index:

$$\text{Anxiety index} = 1 - (\text{open arm time}/5\ \text{min}) + (\text{open arm entry}/\text{total entry}).$$

Rotarod

Following placement of the intrathecal catheters, the rats were trained to walk on a rotating rod (8 rev/min; Rotamex 4/8 device) with a maximal cutoff time of 180 s. Training was initiated by placing the rats on a rotating rod and allowing them to walk on the rotating rod until they either fell off or 180 s was reached. This process was repeated 6 times and the rats were allowed to recover for 24 h before beginning the treatment session. Prior to treatment, the rats were run once on a moving rod in order to establish a baseline value. Saline or t-CNRP1 was administered spinally via the intrathecal catheter. Assessment consisted of placing the rats on the moving

rod and timing until either they fell off or reached a maximum of 180 s. This was repeated 30 min after injection and then every hour for a total time course of 5 h.

Statistical analyses

All data were first tested for a Gaussian distribution using a Shapiro–Wilk test (Graphpad Prism 7 Software). The statistical significance of differences between means was determined by either Student's t test, non-parametric or parametric analysis of variance (ANOVA) followed by post hoc comparisons (Tukey) using GraphPad Prism 7 Software. All behavioral data were analyzed by a non-parametric two-way ANOVA (post hoc: Student–Newman–Keuls) in FlashCalc (Dr. Michael H. Ossipov, University of Arizona, Tucson, AZ, USA). Differences were considered to be significant if $p \leq 0.05$. All data were plotted in GraphPad Prism 7. No outlier data were removed.

RESULTS

t-CNRP1 reverts increased CaV2.2 currents in *Nf1*-edited sensory neurons

We first generated *Nf1*-edited DRG sensory neurons (Fig. 1A) using a CRISPR/Cas9 expressing plasmid together with a gRNA-targeting exon 39 of the rat *Nf1* gene. As described previously (Moutal et al., 2017f), *Nf1* gene editing resulted in increased CaV2.2 currents compared to unedited DRG neurons (Fig. 1). We then asked whether t-CNRP1, a peptide targeting the CRMP2/neurofibromin interaction, could normalize this upregulated CaV2.2 activity. Sensory neurons were treated overnight 10 μM of t-CNRP1 (where t is the trans-acting activator of transcription (TAT) domain of the HIV-1 protein (Schwarze et al., 1999) that facilitates penetration into cells) and then measured Ca^{2+} currents (Fig. 1B). CaV2.2 currents were recorded in the presence of blockers of all other voltage-gated calcium channels in DRGS (see Methods). Under these conditions, t-CNRP1, reversed the increase in Ca^{2+} currents induced by *Nf1* gene editing (Fig. 1C) to the level of non-edited DRG neurons (dotted line, Fig. 1C). These results suggest a role for the CRMP2–neurofibromin interface in increasing CaV2.2 functions in NF1.

t-CNRP1 reverts increased TTX-S Na^+ currents in *Nf1*-edited sensory neurons

Our recent report demonstrated an increase in total Na^+ currents, mostly TTX-S voltage-gated Na^+ channels in sensory neurons isolated from mice following intrathecal editing with CRISPR/Cas9 with a gRNA-targeting exon 39 of *Nf1* (Moutal et al., 2017f), thereby implicating neurofibromin as a possible regulator of Na^+ channels. Our earlier work had shown that CRMP2 plays a role in regulating TTX-S current density through NaV1.7 channels (Dustrude et al., 2016, 2017; Moutal et al., 2017c). Consequently, here we tested if perturbing the CRMP2–neurofibromin interface could affect Na^+ channel dysregulation. Total (Fig. 2A), TTX-S (Fig. 2B) and TTX-R (Fig. 2C) Na^+ currents were increased in *Nf1*-edited sensory neurons compared to unedited neurons. Targeting the CRMP2/neurofibromin interface with t-CNRP1 normalized the increased total Na^+ current density to the level of unedited DRG neurons (Fig. 2D). This effect was due to t-CNRP1-mediated normalization of TTX-S, but not TTX-R, Na^+ currents (Fig. 2D). These results show that the CRMP2/neurofibromin interface regulates Na^+ current density.

The activation V_{50}, the half-inactivated potential for activation of TTX-S currents was -27.2 ± 0.7 mV in control neurons, 30.0 ± 0.3 mV in cells with *Nf1* gRNA, and 24.7 ± 2.1 mV in cells with *Nf1* gRNA treated with 10 μM t-CNRP1 (Table 1). Although the activation V_{50} in cells treated with t-CNRP1 represented a statistically significant difference compared to *Nf1*-edited neurons ($n = 11$ cells, $p < 0.05$, one-way ANOVA with Bonferroni's multiple comparison test), the ~6 mV shift in hyperpolarization reflected a normalization to the activation V_{50} of control cells. For inactivation of TTX-S

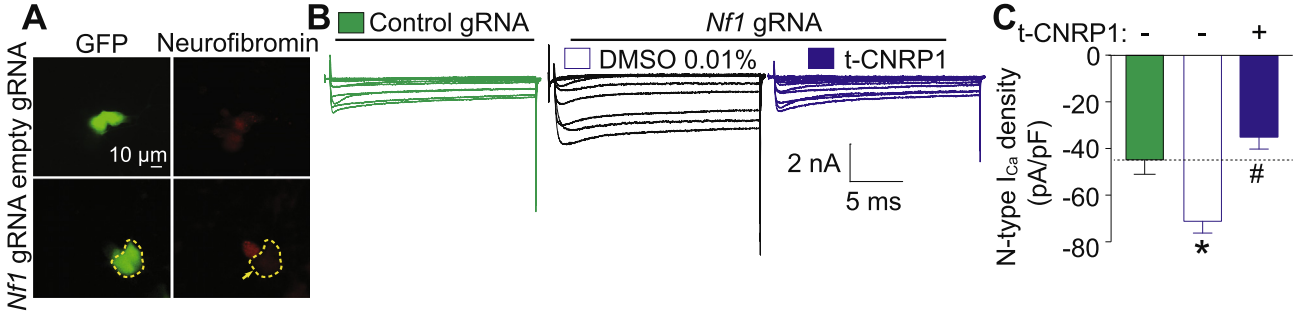

Fig. 1. Increased Ca^{2+} currents in Nf1–edited sensory neurons are normalized by t-CNRP1. (A) Representative micrograph showing neurofibromin levels in DRG neurons transfected with either pSpCas9(BB)-2A-GFP (control gRNA) or pSpCas9(BB)-2A-GFP-Nf1 gRNA plasmids. GFP fluorescence identifies transfected neurons. In this experiment, neuron without GFP has robust expression of neurofibromin, whereas the adjacent neuron with GFP fluorescence (circled) demonstrates significantly decreased neurofibromin expression (marked by an arrow). Scale bar = 10 μm. (B) Representative family of current traces are illustrated for neurons transfected with control or *Nf1* gRNA and treated with 10uM t-CNRP1 or DMSO 0.01%. (C) Peak CaV2.2 current density, at + 10 mV, in DRG neurons unedited or transfected by *Nf1* gRNA containing plasmid and treated with 10 μM t-CNRP1 or DMSO 0.01%. Line shows peak CaV.2.2 current level in *Nf1*-unedited DRG neurons. Mean ± s.e.m., asterisks denote statistical significance compared with 0.01% DMSO-treated cells ($p < 0.05$, non-parametric one-way ANOVA). Recordings are from small and medium DRG neurons.

currents, the trend of a depolarization shift in V_{50} of ~12.6 mV observed in *Nf1* gRNA versus control neurons was restored by t-CNRP1 treatment to V_{50} values observed in control cells (Table 1). For TTX-R currents, the ~7 mV shift in hyperpolarization caused by *Nf1* editing was negated by t-CNRP1 treatment which brought the activation V_{50} to levels observed in control cells ($p < 0.05$, one-way ANOVA with Bonferroni's multiple comparison test) (Table 1). No significant difference for the inactivation of TTX-R currents was detected ($p < 0.05$, one-way ANOVA with Bonferroni's multiple comparison test). This indicates that t-CNRP1 normalizes the biophysical properties of TTX-S and TTX-R currents after *Nf1* editing in DRG neurons.

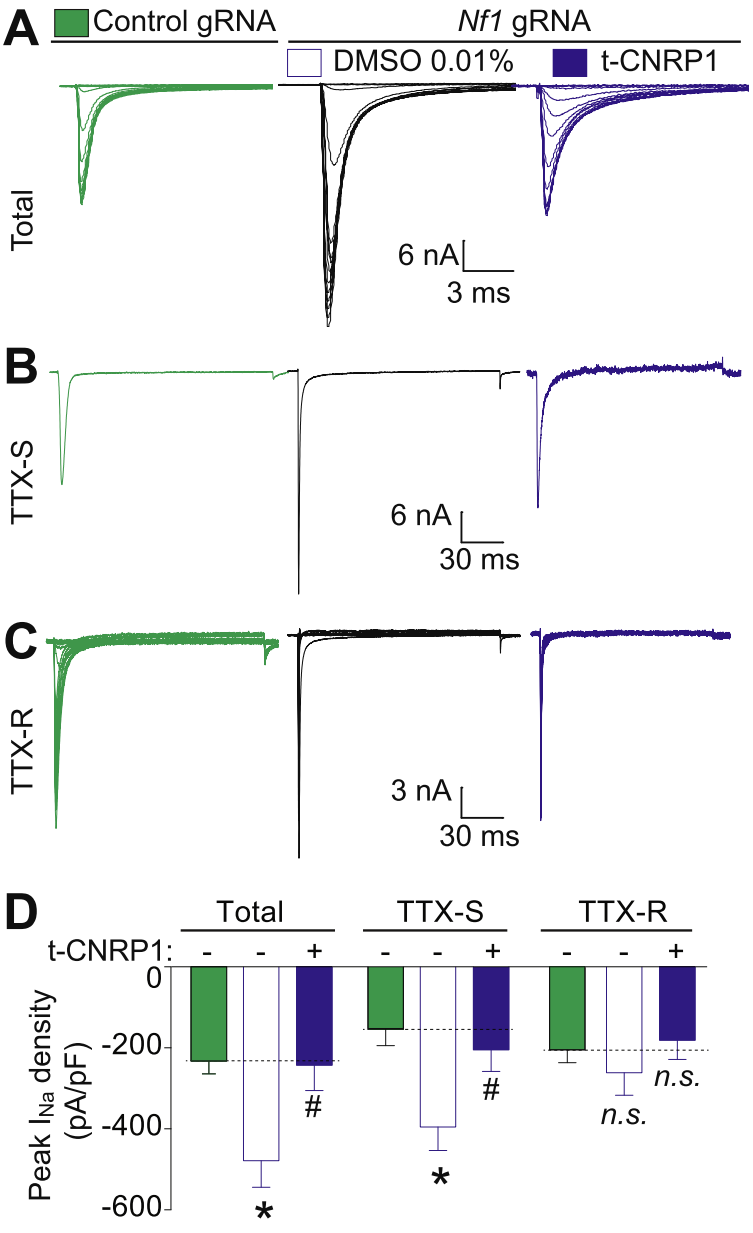

Fig. 2. Increased total and TTX-S Na^+ currents in Nf1-edited sensory neurons are normalized by t-CNRP1. Representative family of total (A), tetrodotoxin-sensitive (TTX-S) (B), and TTX-resistant (TTX-R) (C) Na^+ current traces are illustrated for Nf1-edited sensory neurons and treated with 10 μM t-CNRP1 or DMSO 0.01% compared to unedited neurons. (D) Peak current density for Total, TTX-S or TTX-R Na^+ current density in unedited DRG neurons or transfected by *Nf1* gRNA containing plasmid and treated with either 10 μM t-CNRP1 or DMSO 0.01%. Line shows peak current level in DRG neurons transfected with the empty plasmid. Mean ± s.e.m., asterisks denote statistical significance compared with 0.01% DMSO-treated cells ($p < 0.05$, non-parametric one-way ANOVA). n.s., not-significant; $P > 0.05$; non-parametric one way ANOVA. Recordings are from small and medium DRG neurons.

t-CNRP1 reduces CaV2.2 and NaV1.7 surface localization in *Nf1*-edited sensory neurons

CRMP2 promotes surface expression of CaV2.2 (Brittain et al., 2009, 2011, 2012; Francois-Moutal et al., 2015) and NaV1.7 (Dustrude et al., 2013, 2016, 2017). Since t-CNRP1 decreased both Ca^{2+} and Na^+ current densities, we hypothesized that treating *Nf1*-edited sensory neurons with this peptide might reduce the surface expression of CaV2.2 and NaV1.7. After overnight treatment of *Nf1*-edited sensory neurons with 10 μM of t-CNRP1, CaV2.2 and NaV1.7 were immunostained. We used confocal imaging to analyze the localization in close vicinity of the membrane for CaV2.2 and NaV1.7 in *Nf1*-edited DRG neurons (identified by GFP expression) (Fig. 3A). We found that t-CNRP1 decreased the surface localization of both CaV2.2 and NaV1.7 (Fig. 3) compared to control (0.01% DMSO) neurons. Thus, the decreased Ca^{2+} and Na^+ current densities induced by t-CNRP1 are related to a decreased surface expression of these channels.

t-CNRP1 reverts the increased excitability in *Nf1*-edited sensory neurons

NaV1.7 is a voltage-gated Na^+ channel participating in the upstroke of action potential firing by sensory neurons (Dib-Hajj et al., 2013). In *Nf1*-edited DRG neurons, we recently reported that the increase in Na^+ currents is related to a decreased rheobase and increased action potential firing (Moutal et al., 2017f). Thus, we tested if t-CNRP1 could reduce *Nf1*-edited DRG neuron excitability. *Nf1*-edited neurons were treated overnight with 10 μM of t-CNRP1 or vehicle (0.01% DMSO) and neuronal excitability was measured in ramp and step protocols (Fig. 4A–D). t-CNRP1 treatment of *Nf1*-edited sensory neurons reversed the increased action potential (AP) firing (Fig. 4A–D) to the level of non-edited DRG neurons (Fig. 4E). The rheobase of t-CNRP1-treated *Nf1*-edited neurons was more than doubled versus that in vehicle-treated cells (0.01% DMSO) (Fig. 4F). The resting membrane potential, which is not altered by *Nf1* gene editing (Moutal et al., 2017f), was not changed by t-CNRP1. These data show the CRMP2–neurofibromin interface is involved in increased excitability manifest as in increase AP and a decrease in rheobase in *Nf1*-edited DRG sensory neurons.

Table 1. Boltzmann's parameters for the activation and inactivation of tetrodotoxin-sensitive (TTX-S) and resistant (TTX-R) I_{Na} in control and *Nf1* sgRNA-transfected dorsal root ganglion neurons

	$V_{0.5}$ (mV)	*k*
TTX-S		
INa activation		
Control (*n* = 9)	−27.2 ± 0.7	5.0 ± 0.3
Nf1 gRNA (*n* = 11)	−30.0 ± 0.3	4.3 ± 0.3
Nf1 gRNA + t-CNRP1 (*n* = 11)	−24.7 ± 2.1[a]	7.0 ± 1.3
INa inactivation		
Control (*n* = 9)	−64.0 ± 3.2	7.7 ± 1.5
Nf1 gRNA (*n* = 11)	−51.4 ± 7.0	17.2 ± 1.8[b]
Nf1 gRNA + t-CNRP1 (*n* = 11)	−68.3 ± 1.3[a]	13.5 ± 0.7
TTX-R		
INa activation		
Control (*n* = 9)	−20.0 ± 0.7	7.8 ± 0.7
Nf1 gRNA (*n* = 11)	−26.9 ± 0.7[b]	5.8 ± 0.2
Nf1 gRNA + t-CNRP1 (*n* = 11)	−19.9 ± 1.4[a]	5.8 ± 0.4
INa inactivation		
Control (*n* = 9)	−30.0 ± 2.4	5.6 ± 1.6
Nf1 gRNA (*n* = 11)	−36.3 ± 5.1	8.2 ± 2.6
Nf1 gRNA + t-CNRP1 (*n* = 11)	−43.9 ± 7.1	15.7 ± 3.5 [a]

[a] $p < 0.05$ vs Nf1 sgRNA (One-way ANOVA with Bonferroni's multiple comparison test).

[b] $p < 0.05$ vs control (One-way ANOVA with Bonferroni's multiple comparison test).

t-CNRP1 reverses Nf1-editing-induced thermal hyperalgesia in both male and female rats

In vivo Nf1 gene editing (Fig. 5A) leads to the development of thermal hyperalgesia (Moutal et al., 2017f), setting up a causal relationship between neurofibromin and pain. Our *in vitro* data show that t-CNRP1 treatment of *Nf1*-edited cells normalizes the increased CaV2.2 and NaV1.7 currents as well as sensory neuronal excitability. Thus, we tested if t-CNRP1 could be beneficial in this new model of NF1 pain. Intraperitoneal injection (30 mg/kg) of t-CNRP1 reversed the decreased paw withdrawal latency after 30 min, an effect that lasted for 4 h in males (Fig. 5B) and for 3.5 h in females (Fig. 5C). Although, some early time points demonstrated paw withdrawal latency above the baseline of unedited rats, this effect was not significant. Injecting t-CNRP1 in non-edited rats (control gRNA) did not elicit any analgesia. t-CNRP1 did not change the thermal withdrawal threshold in control animals where *Nf1* is intact.

To rule out possible off-target effects of the CNRP1 peptide, we tested whether t-CNRP1 could be involved in motor coordination (rotarod) or anxiety (EPM). To ensure availability of the peptide in the spinal cord, we administered the drug intrathecally in these experiments. Intrathecal injection of t-CNRP1 (30 μg/5μl) had no effect on the latency to fall (Fig. 6A) or on the anxiety index (Fig. 6B). Thus, targeting the CRMP2–neurofibromin interface specifically reduces NF1-related pain. Another inference from the behavioral results is that t-CNRP1 is likely acting on DRG neurons and not on motor neurons.

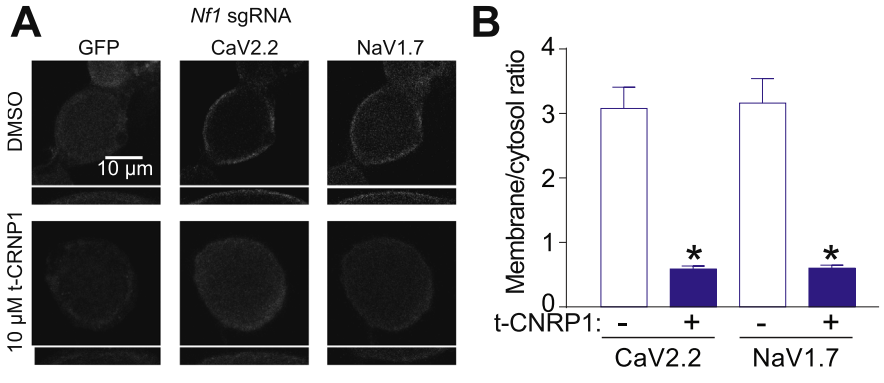

Fig. 3. CaV2.2 and NaV1.7 surface localization is decreased by t-CNRP1 in Nf1-edited sensory neurons. (A) Representative micrographs of CaV2.2 and NaV1.7 localization in Nf1-edited DRG neurons (identified by GFP expression) treated with 10 μM t-CNRP1 or DMSO 0.01% ($n = 12$ per condition). Scale bar = 10 μm (B) quantification of the relative membrane localization of CaV2.2 and NaV1.7 (compared to cytosol) in Nf1-edited DRG neurons treated with 10 μM t-CNRP1 or DMSO 0.01% ($n = 11$ per condition). Insets in panels A and B represent 2X magnified versions of the annular regions of staining on the cells.

DISCUSSION

The work presented here reveals additional insights into NF1-related pain. We had previously identified CRMP2 expression to be required for NF1-related pain (Moutal et al., 2017a) and had reported that the CRMP2–neurofibromin interaction was an important mediator of post-surgical, inflammatory and neuropathic nociceptive behaviors (Moutal et al., 2017f). The CRMP2–neurofibromin interaction likely regulates CRMP2 functions by (i) modifying CRMP2's post-translational state (Patrakitkomjorn et al., 2008; Moutal et al., 2017f) and (ii) controlling CRMP2's interactome (Moutal et al., 2017f). These observations suggested that the loss of protein–protein interactions (PPIs) between CRMP2 and neurofibromin might explain NF1-related pain. We thus tested whether targeting the CRMP2–neurofibromin interface could normalize ion channel dysregulation and nociceptive behaviors in a CRISPR/Cas9-induced *in vitro* and *in vivo* model of NF1-related pain.

A CRMP2-derived peptide (CNRP1) was designed based on CRMP2's interaction domain with neurofibromin. We previously found that this peptide inhibited CRMP2's interaction with CaV2.2, neurofibromin, and syntaxin 1A. A cell-penetrant version of this peptide (t-CNRP1) inhibited CaV2.2 and NaV1.7 currents in *Nf1*-edited neurons. CRMP2 regulation of the NaV1.7 TTX-S Na^+ channel was dependent on the CRMP2's phosphorylation and SUMOylation state (Dustrude et al., 2013, 2016, 2017). The results reported here

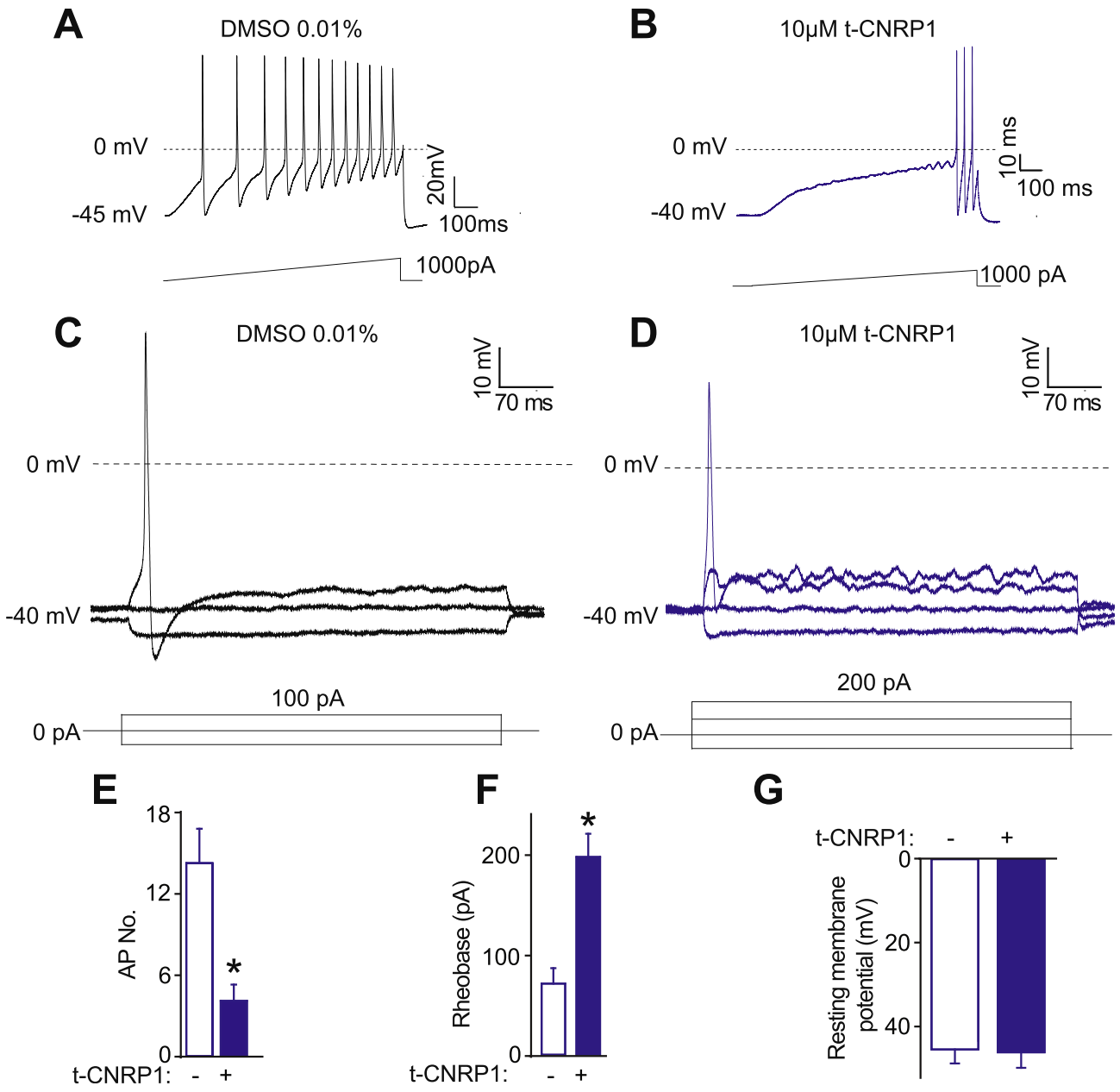

Fig. 4. Hyperexcitability in Nf1-edited sensory neurons is controlled by t-CNRP1. Representative recordings in response to a step of depolarizing current-evoked action potentials (APs) in Nf1-edited sensory neurons treated with (A) DMSO 0.01% or (B) 10 μM t-CNRP1. Representative recordings in response to various steps of depolarizing current to measure rheobase in Nf1-edited sensory neurons treated with (C) DMSO 0.01% or (D) 10 μM t-CNRP1. Rheobase is the current required for eliciting the first AP. Summary of the number of action potentials (E), rheobase (F), and resting membrane potentials (G) recorded from Nf1-edited DRG neurons treated with 10 μM t-CNRP1 or DMSO 0.01%. Recordings are from small and medium DRG neurons.

appear independent of these modifications and identify a novel pathway of NaV1.7 regulation by the CRMP2–neurofibromin interface.

How does the CRMP2–neurofibromin interaction bestow regulation on NaV1.7?

One possibility is via CRMP2's interaction with syntaxin 1A. We previously reported that t-CNRP1 inhibits the CRMP2/syntaxin 1A interaction [11]. Syntaxin 1A is part of the SNARE (Soluble N-ethylmaleimide-sensitive-factor Attachment REceptor)–protein complex mediating vesicular fusion at the synapse (Fergestad et al., 2001). Syntaxin 1A can interact with synaptotagmin, a protein known to interact with voltage-gated Na^+ channels (Sampo et al., 2000) and possibly with NaV1.7 (Kanellopoulos et al., 2017). This CRMP2–Syntaxin 1A–synaptotagmin–NaV1.7 PPI complex might coordinate NaV1.7 membrane localization. By disrupting these interactions, t-CNRP1 could trigger the internalization of the Na^+ channel. CRMP2 can also, in its unphosphorylated state, bind to tubulin and promote axonal growth

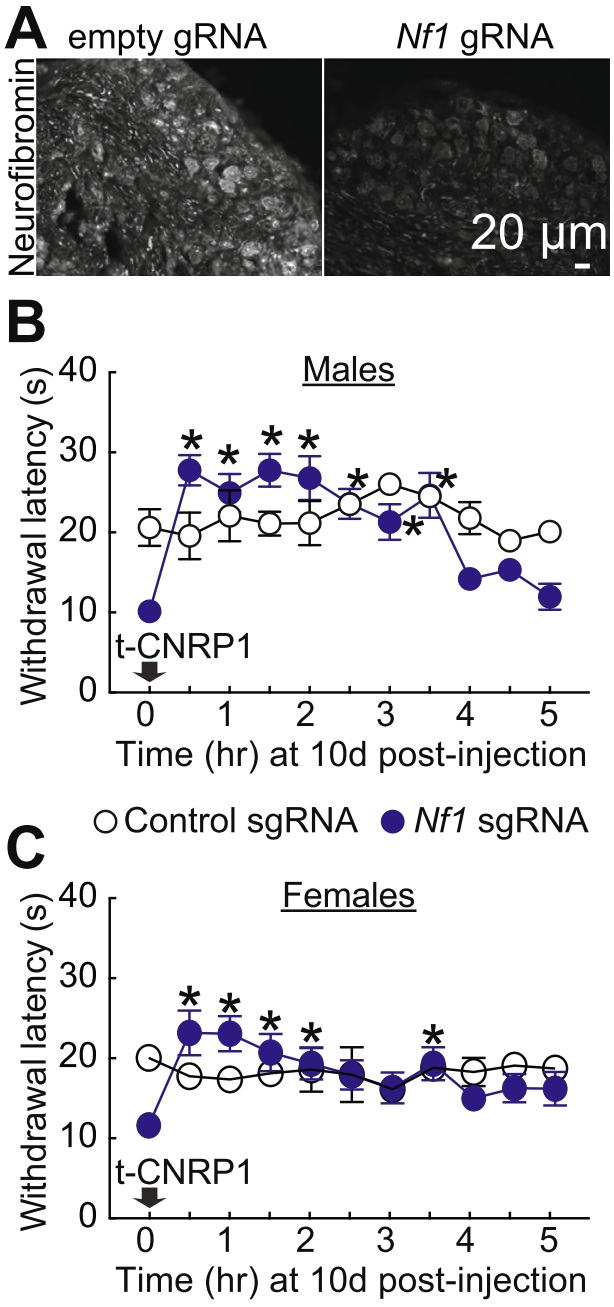

Fig. 5. NF1-related thermal hyperalgesia can be reverted by t-CNRP1. (A) Micrographs of a 10-µm section of adult DRG from animals having received intrathecal injection of either Nf1 gRNA containing or control gRNA plasmid (day 10) immunostained with neurofibromin antibody as indicated. Scale bar = 20 µm. Thermal hyperalgesia (paw withdrawal latency) of rats, 10 days after *in vivo* transfection with control or Nf1 gRNA containing plasmids. Paw withdrawal latency was followed for 5 h after intraperitoneal injection of t-CNRP1 (30 mg/kg). Paw withdrawal latency threshold was increased by t-CNRP1 injection in *Nf1*-edited males (B) and females (C) rats (n = 6 each). $^{*}P < 0.05$ versus control gRNA, 2-way ANOVA with a Student–Newman–Keuls post hoc test. Error bars represent mean ± s.e.m.

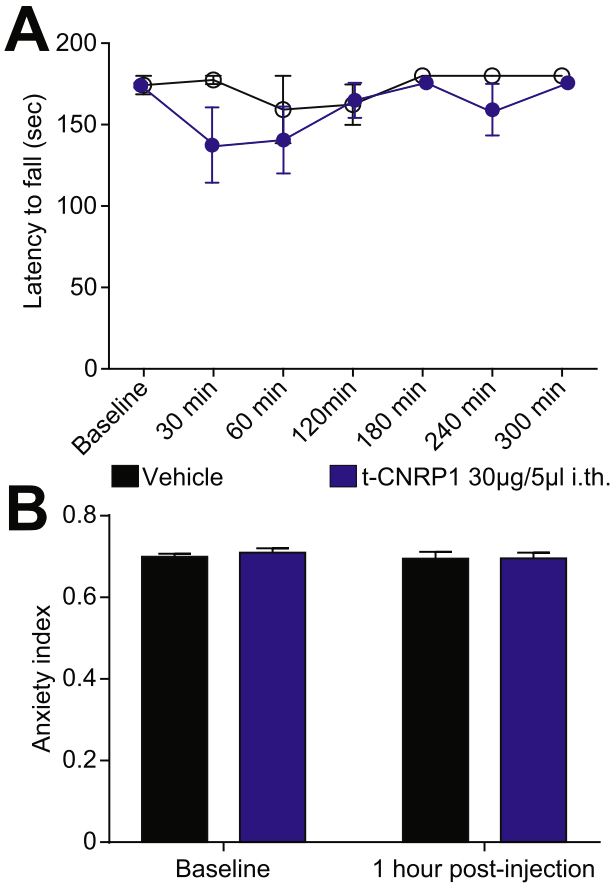

Fig. 6. Comparison of anxiety index following targeted intrathecal editing of *Nf1 in vivo*. Spinal administration of t-CNRP1 (30 µg/5µl) or vehicle (0.9% saline) was evaluated for motor deficits using the rotarod performance test. No significant difference was measured between t-CNRP1-treated and vehicle-treated animals, 2-way ANOVA with a Student–Newman–Keuls post hoc test. (B) The anxiety index, an integrated measure of times and entries into the arms of the elevated plus maze, was not different between vehicle (0.01% DMSO) and t-CNRP1 (30 µg/5 µl), before and after injection. Values are shown as mean ± s.e.m (n = 6 each).

(Gu and Ihara, 2000; Fukata et al., 2002). CRMP2 phosphorylation by Cdk5 (Uchida et al., 2005) or Fyn (Uchida et al., 2009) results in a decrease in CRMP2 binding to tubulin and inhibits axonal elongation. Since we found NaV1.7 function to be protected by CRMP2 phosphorylation by Cdk5 and inhibited after CRMP2 phosphorylation by Fyn (Dustrude et al., 2016), the fraction of CRMP2-regulating NaV1.7 is unlikely to interact with tubulin. This rules out a potential function of t-CNRP1 in altering CRMP2 function on axonal growth.

In addition, this PPI complex, identified elsewhere (Dustrude et al., 2016; Moutal et al., 2017e), sets up a possible coupling of NaV1.7 activity to neurotransmitter release. Support for this comes from previous observations that t-CNRP1 inhibits the release of the nociceptive calcitonin gene-related peptide (CGRP) (Moutal et al., 2017e), a transmitter that is increased in *Nf1*-edited rats and $Nf1^{+/-}$ mice (Hingtgen et al., 2006; Moutal et al., 2017a). A function for NaV1.7 in CGRP release was suggested by the use of voltage-gated Na^{+} channel activating ciguatoxins (Touska et al., 2017). These toxins elicited a strong CGRP release, ~40% of which was dependent on NaV1.7 activation (Touska et al., 2017). Thus, CRMP2's interface with neurofibromin may recruit CaV2.2, NaV1.7 and the SNARE complex to link the

trafficking function of these channels to neuropeptide release in NF1-related pain.

CRMP2 forms a tetramer in solution (Dustrude et al., 2017; Francois-Moutal et al., 2015; Moutal et al., 2016c; Wang and Strittmatter, 1997; Stenmark et al., 2007; Touska et al., 2017) and thus presents multiple copies of PPI sites available to build potential PPI modules. A closer look at the sequence of CRMP2 reveals clues as to the organization of key binding motifs that may participate in a concerted fashion to link trafficking to transmitter release. Key CRMP2 domains include: (*i*) residues 460–474 that interact with neurofibromin or syntaxin 1A (Moutal et al., 2017e); (*ii*) residue 484–498 (Brittain et al., 2011), later refined as 484–489 (Moutal et al., 2017d) that mediates its binding to CaV2.2; (*iii*) residues 466–490 that bind to tubulin (Niwa et al., 2017); and (*iv*) residues 422–572 that interact with the molecular motor kinesin1 that allows vesicular transport toward the synapse (Kimura et al., 2005). Because of its tetrameric structure, CRMP2 could be a scaffold between all of these proteins and contribute to the assembly of a neurotransmitter release platform. CRMP2 interactions with tubulin and kinesin1 may coordinate the peregrination of CaV2.2 and NaV1.7 to the synapse, possibly explaining their respective increased current densities. Also, CRMP2's interaction with syntaxin 1A, which is augmented when CRMP2's interaction with neurofibromin is lost (Moutal et al., 2017e), could aid in docking of synaptic vesicles directly to these channels. Syntaxin 1A's interaction with synaptotagmin could, in turn, link CRMP2, CaV2.2 and NaV1.7 together. Such a model would accommodate a potential interplay between these channels. NaV1.7 activation would cause local membrane depolarization, readily opening CaV2.2. The release of the neurotransmitter containing vesicles, directly docked between both channels through CRMP2 and syntaxin 1A, would then be triggered by the influx of Ca^{2+} ions thus eliciting a nociceptive signal. If true, it follows that an increased formation of such a signaling platform could underlie the hyperalgesia observed upon *Nf1* gene editing.

In summary, our findings identify a novel signaling hub, designated here as a neurotransmitter release platform that positions ion channels (i.e., CaV2.2, NaV1.7) adjacent to the release machinery (i.e., syntaxin 1A, synaptotagmin) for rapid nociceptive signal transmission. In this platform, neurofibromin interacts with CRMP2 to prevent recruitment of syntaxin 1A and CaV2.2, thus leading to block of CGRP and a reduction in pain behaviors. Our findings support future pharmacological targeting of the CRMP2/neurofibromin interface for NF1-related pain relief.

ACKNOWLEDGMENTS

This work was supported by National Institutes of Health awards (1R01NS098772 from the National Institute of Neurological Disorders and Stroke and 1R01DA042852 from the National Institute on Drug Abuse); a Neurofibromatosis New Investigator Award from the Department of Defense Congressionally Directed Military Medical Research and Development Program (NF1000099); and a Children's Tumor Foundation NF1 Synodos award (2015-04-009A) to R.K and a General Program of the National Science Foundation of China grant (no. 81571231) to S.L. A.M. was supported by a Young Investigator's Award from the Children's Tumor Foundation (2015-01-011).

CONFLICT OF INTEREST

The authors declare that they have no conflict of interest.

REFERENCES

Bicudo NP, de Menezes Neto BF, da Silva de Avo LR, Germano CM, Melo DG (2016) Quality of life in adults with neurofibromatosis 1 in Brazil. J Genet Couns 25:1063–1074.

Brittain JM, Piekarz AD, Wang Y, Kondo T, Cummins TR, Khanna R (2009) An atypical role for collapsin response mediator protein 2 (CRMP-2) in neurotransmitter release via interaction with presynaptic voltage-gated calcium channels. J Biol Chem 284:31375–31390.

Brittain JM, Duarte DB, Wilson SM, Zhu W, Ballard C, Johnson PL, Liu N, Xiong W, et al. (2011) Suppression of inflammatory and neuropathic pain by uncoupling CRMP-2 from the presynaptic Ca (2)(+) channel complex. Nat Med 17:822–829.

Brittain JM, Wang Y, Eruvwetere O, Khanna R (2012) Cdk5-mediated phosphorylation of CRMP-2 enhances its interaction with CaV2.2. FEBS Lett 586:3813–3818.

Chew LA, Khanna R (2018) CRMP2 and voltage-gated ion channels: potential roles in neuropathic pain. Neuronal Signaling 2:16.

Chi XX, Schmutzler BS, Brittain JM, Wang Y, Hingtgen CM, Nicol GD, Khanna R (2009) Regulation of N-type voltage-gated calcium channels (Cav2.2) and transmitter release by collapsin response mediator protein-2 (CRMP-2) in sensory neurons. J Cell Sci 122:4351–4362.

Choe W, Messinger RB, Leach E, Eckle VS, Obradovic A, Salajegheh R, Jevtovic-Todorovic V, Todorovic SM (2011) TTA-P2 is a potent and selective blocker of T-type calcium channels in rat sensory neurons and a novel antinociceptive agent. Mol Pharmacol 80:900–910.

Crawford HA, Barton B, Wilson MJ, Berman Y, McKelvey-Martin VJ, Morrison PJ, North KN (2015) The impact of neurofibromatosis type 1 on the health and wellbeing of australian adults. J Genet Couns 24:931–944.

Creange A, Zeller J, Rostaing-Rigattieri S, Brugieres P, Degos JD, Revuz J, Wolkenstein P (1999) Neurological complications of neurofibromatosis type 1 in adulthood. Brain 122:473–481.

Dib-Hajj SD, Yang Y, Black JA, Waxman SG (2013) The Na(V)1.7 sodium channel: from molecule to man. Nat Rev Neurosci 14:49–62.

Drouet A, Wolkenstein P, Lefaucheur JP, Pinson S, Combemale P, Gherardi RK, Brugieres P, Salama J, et al. (2004) Neurofibromatosis 1-associated neuropathies: a reappraisal. Brain 127:1993–2009.

Duan JH, Hodgdon KE, Hingtgen CM, Nicol GD (2014) N-type calcium current, Cav2.2, is enhanced in small-diameter sensory neurons isolated from Nf1+/− mice. Neuroscience 270:192–202.

Dustrude ET, Wilson SM, Ju W, Xiao Y, Khanna R (2013) CRMP2 protein SUMOylation modulates NaV1.7 channel trafficking. J Biol Chem 288:24316–24331.

Dustrude ET, Moutal A, Yang X, Wang Y, Khanna M, Khanna R (2016) Hierarchical CRMP2 posttranslational modifications control NaV1.7 function. PNAS 113:E8443–E8452.

Dustrude ET, Perez-Miller S, Francois-Moutal L, Moutal A, Khanna M, Khanna R (2017) A single structurally conserved SUMOylation site in CRMP2 controls NaV1.7 function. Channels 11:316–328.

Esposito T, Piluso G, Saracino D, Uccello R, Schettino C, Dato C, Capaldo G, Giugliano T, et al. (2015) A novel diagnostic method

to detect truncated neurofibromin in neurofibromatosis 1. J Neurochem 135:1123–1128.
Fergestad T, Wu MN, Schulze KL, Lloyd TE, Bellen HJ, Broadie K (2001) Targeted mutations in the syntaxin H3 domain specifically disrupt SNARE complex function in synaptic transmission. J Neurosci 21:9142–9150.
Ferner RE (2007) Neurofibromatosis 1 and neurofibromatosis 2: a twenty first century perspective. Lancet Neurol 6:340–351.
Ferner RE, Thomas M, Mercer G, Williams V, Leschziner GD, Afridi SK, Golding JF (2017) Evaluation of quality of life in adults with neurofibromatosis 1 (NF1) using the impact of NF1 on quality of life (INF1-QOL) questionnaire. Health Quality Life Outcomes 15:34.
Francois-Moutal L, Wang Y, Moutal A, Cottier KE, Melemedjian OK, Yang X, Wang Y, Ju W, et al. (2015) A membrane-delimited N-myristoylated CRMP2 peptide aptamer inhibits CaV2.2 trafficking and reverses inflammatory and postoperative pain behaviors. Pain 156:1247–1264.
Fukata Y, Itoh TJ, Kimura T, Menager C, Nishimura T, Shiromizu T, Watanabe H, Inagaki N, et al. (2002) CRMP-2 binds to tubulin heterodimers to promote microtubule assembly. Nat Cell Biol 4:583–591.
Goshima Y, Nakamura F, Strittmatter P, Strittmatter SM (1995) Collapsin-induced growth cone collapse mediated by an intracellular protein related to UNC-33. Nature 376:509–514.
Gu Y, Ihara Y (2000) Evidence that collapsin response mediator protein-2 is involved in the dynamics of microtubules. J Biol Chem 275:17917–17920.
Hargreaves K, Dubner R, Brown F, Flores C, Joris J (1988) A new and sensitive method for measuring thermal nociception in cutaneous hyperalgesia. Pain 32:77–88.
Hingtgen CM, Roy SL, Clapp DW (2006) Stimulus-evoked release of neuropeptides is enhanced in sensory neurons from mice with a heterozygous mutation of the Nf1 gene. Neuroscience 137:637–645.
Huynh TN, Krigbaum AM, Hanna JJ, Conrad CD (2011) Sex differences and phase of light cycle modify chronic stress effects on anxiety and depressive-like behavior. Behav Brain Res 222:212–222.
Ju W, Li Q, Allette YM, Ripsch MS, White FA, Khanna R (2012) Suppression of pain-related behavior in two distinct rodent models of peripheral neuropathy by a homopolyarginine-conjugated CRMP2 peptide. J Neurochem 124:869–879.
Kamata T, Subleski M, Hara Y, Yuhki N, Kung H, Copeland NG, Jenkins NA, Yoshimura T, et al. (1998) Isolation and characterization of a bovine neural specific protein (CRMP-2) cDNA homologous to unc-33, a C. elegans gene implicated in axonal outgrowth and guidance. Brain Res Mol Brain Res 54:219–236.
Kanellopoulos AH, Koenig J, Huang H, Pyrski M, Millet Q, Lolignier S, Morohashi T, Gossage SJ, et al. (2017) Mapping protein interactions of sodium channel NaV1.7 using epitope-tagged gene targeted mice. BioRxiv.
Kimura T, Watanabe H, Iwamatsu A, Kaibuchi K (2005) Tubulin and CRMP-2 complex is transported via Kinesin-1. J Neurochem 93:1371–1382.
Kodra Y, Giustini S, Divona L, Porciello R, Calvieri S, Wolkenstein P, Taruscio D (2009) Health-related quality of life in patients with neurofibromatosis type 1. A survey of 129 Italian patients. Dermatology 218:215–220.
Lin YL, Hsueh YP (2008) Neurofibromin interacts with CRMP-2 and CRMP-4 in rat brain. Biochem Biophys Res Commun 369:747–752.
Mintz IM, Venema VJ, Swiderek KM, Lee TD, Bean BP, Adams ME (1992) P-type calcium channels blocked by the spider toxin omega-Aga-IVA. Nature 355:827–829.
Moutal A, Chew LA, Yang X, Wang Y, Yeon SK, Telemi E, Meroueh S, Park KD, et al. (2016a) (S)-lacosamide inhibition of CRMP2 phosphorylation reduces postoperative and neuropathic pain behaviors through distinct classes of sensory neurons identified by constellation pharmacology. Pain 157:1448–1463.
Moutal A, Eyde N, Telemi E, Park KD, Xie JY, Dodick DW, Porreca F, Khanna R (2016b) Efficacy of (S)-lacosamide in preclinical models of cephalic pain. Pain Rep 1(1):pii: e565.
Moutal A, Francois-Moutal L, Perez-Miller S, Cottier K, Chew LA, Yeon SK, Dai J, Park KD, et al. (2016c) (S)-Lacosamide binding to collapsin response mediator protein 2 (CRMP2) regulates CaV2.2 activity by subverting its phosphorylation by Cdk5. Mol Neurobiol 53:1959–1976.
Moutal A, Cai S, Luo S, Voisin R, Khanna R (2017a) CRMP2 is necessary for neurofibromatosis type 1 related pain. Channels (Austin) 12(1):47–50.
Moutal A, Dustrude ET, Khanna R (2017b) Sensitization of ion channels contributes to central and peripheral dysfunction in neurofibromatosis Type 1. Mol Neurobiol 54:3342–3349.
Moutal A, Dustrude ET, Largent-Milnes TM, Vanderah TW, Khanna M, Khanna R (2017c) Blocking CRMP2 SUMOylation reverses neuropathic pain. Mol Psychiatry. https://doi.org/10.1038/mp.2017.117.
Moutal A, Li W, Wang Y, Ju W, Luo S, Cai S, Francois-Moutal L, Perez-Miller S, et al. (2017d) Homology-guided mutational analysis reveals the functional requirements for antinociceptive specificity of collapsin response mediator protein 2-derived peptides. Br J Pharmacol. https://doi.org/10.1111/bph.13737.
Moutal A, Wang Y, Yang X, Ji Y, Luo S, Dorame A, Bellampalli SS, Chew LA, et al. (2017e) Dissecting the role of the CRMP2-neurofibromin complex on pain behaviors. Pain.
Moutal A, Yang X, Li W, Gilbraith KB, Luo S, Cai S, Francois-Moutal L, Chew LA, et al. (2017f) CRISPR/Cas9 editing of Nf1 gene identifies CRMP2 as a therapeutic target in neurofibromatosis type 1 (NF1)-related pain that is reversed by (S)-lacosamide. Pain 158(12):2301–2319.
Newcomb R, Szoke B, Palma A, Wang G, Chen X, Hopkins W, Cong R, Miller J, et al. (1998) Selective peptide antagonist of the class E calcium channel from the venom of the tarantula Hysterocrates gigas. Biochemistry 37:15353–15362.
Niwa S, Nakamura F, Tomabechi Y, Aoki M, Shigematsu H, Matsumoto T, Yamagata A, Fukai S, et al. (2017) Structural basis for CRMP2-induced axonal microtubule formation. Sci Rep 7:10681.
Patrakitkomjorn S, Kobayashi D, Morikawa T, Wilson MM, Tsubota N, Irie A, Ozawa T, Aoki M, et al. (2008) Neurofibromatosis type 1 (NF1) tumor suppressor, neurofibromin, regulates the neuronal differentiation of PC12 cells via its associating protein, CRMP-2. J Biol Chem 283:9399–9413.
Piekarz AD, Due MR, Khanna M, Wang B, Ripsch MS, Wang R, Meroueh SO, Vasko MR, et al. (2012) CRMP-2 peptide mediated decrease of high and low voltage-activated calcium channels, attenuation of nociceptor excitability, and anti-nociception in a model of AIDS therapy-induced painful peripheral neuropathy. Mol Pain 8:54.
Ran FA, Hsu PD, Wright J, Agarwala V, Scott DA, Zhang F (2013) Genome engineering using the CRISPR-Cas9 system. Nat Protoc 8:2281–2308.
Riklin E, Talaei-Kheoi M, Merker VL, Sheridan MR, Jordan JT, Plotkin SR, Vranceanu AM (2017) First report of factors associated with satisfaction in patients with neurofibromatosis. Am J Med Genet Part A 173:671–677.
Roy ML, Narahashi T (1992) Differential properties of tetrodotoxin-sensitive and tetrodotoxin-resistant sodium channels in rat dorsal root ganglion neurons. J Neurosci 12:2104–2111.
Sampo B, Tricaud N, Leveque C, Seagar M, Couraud F, Dargent B (2000) Direct interaction between synaptotagmin and the intracellular loop I-II of neuronal voltage-sensitive sodium channels. PNAS 97:3666–3671.
Schwarze SR, Ho A, Vocero-Akbani A, Dowdy SF (1999) In vivo protein transduction: delivery of a biologically active protein into the mouse. Science 285:1569–1572.
Scroggs RS, Fox AP (1992) Calcium current variation between acutely isolated adult rat dorsal root ganglion neurons of different size. J Physiol 445:639–658.

Stenmark P, Ogg D, Flodin S, Flores A, Kotenyova T, Nyman T, Nordlund P, Kursula P (2007) The structure of human collapsin response mediator protein 2, a regulator of axonal growth. J Neurochem 101:906–917.

Touska F, Sattler S, Malsch P, Lewis RJ, Reeh PW, Zimmermann K (2017) Ciguatoxins evoke potent CGRP release by activation of voltage-gated sodium channel subtypes NaV1.9, NaV1.7 and NaV1.1. Mar Drugs 15.

Uchida Y, Ohshima T, Sasaki Y, Suzuki H, Yanai S, Yamashita N, Nakamura F, Takei K, et al. (2005) Semaphorin3A signalling is mediated via sequential Cdk5 and GSK3beta phosphorylation of CRMP2: implication of common phosphorylating mechanism underlying axon guidance and Alzheimer's disease. Genes Cells 10:165–179.

Uchida Y, Ohshima TYamashita N, Ogawara M, Sasaki Y, Nakamura F, Goshima Y (2009) Semaphorin3A signaling mediated by Fyn-dependent tyrosine phosphorylation of collapsin response mediator protein 2 at tyrosine 32. J Biol Chem 284:27393–27401.

Wang LH, Strittmatter SM (1997) Brain CRMP forms heterotetramers similar to liver dihydropyrimidinase. J Neurochem 69:2261–2269.

Wang Y, Nicol GD, Clapp DW, Hingtgen CM (2005) Sensory neurons from Nf1 haploinsufficient mice exhibit increased excitability. J Neurophysiol 94:3670–3676.

Wang Y, Brittain JM, Wilson SM, Hingtgen CM, Khanna R (2010a) Altered calcium currents and axonal growth in Nf1 haploinsufficient mice. Transl Neurosci 1:106–114.

Wang Y, Duan JH, Hingtgen CM, Nicol GD (2010b) Augmented sodium currents contribute to enhanced excitability of small diameter capsaicin-sensitive Nf1 + / − mouse sensory neurons. J Neurophysiol.

Wolkenstein P, Zeller J, Revuz J, Ecosse E, Leplege A (2001) Quality-of-life impairment in neurofibromatosis type 1: a cross-sectional study of 128 cases. Arch Dermatol 137:1421–1425.

Wolters PL, Burns KM, Martin S, Baldwin A, Dombi E, Toledo-Tamula MA, Dudley WN, Gillespie A, et al. (2015) Pain interference in youth with neurofibromatosis type 1 and plexiform neurofibromas and relation to disease severity, social-emotional functioning, and quality of life. Am J Med Genet Part A 167A:2103–2113.

Yaksh TL, Rudy TA (1976) Chronic catheterization of the spinal subarachnoid space. Physiol Behav 17:1031–1036.

(Received 20 January 2018, Accepted 4 April 2018)
(Available online 12 April 2018)